The Variable Rotation Period of the Inner Region of Saturn's Plasma Disk

D. A. Gurnett, *et al.*

Science **316**, 442 (2007);
DOI: 10.1126/science.1138562

The Variable Rotation Period of the Inner Region of Saturn's Plasma Disk

D. A. Gurnett,[1] A. M. Persoon,[1] W. S. Kurth,[1] J. B. Groene,[1] T. F. Averkamp,[1] M. K. Dougherty,[2] D. J. Southwood[2,3]

We show that the plasma and magnetic fields in the inner region of Saturn's plasma disk rotate in synchronism with the time-variable modulation period of Saturn's kilometric radio emission. This relation suggests that the radio modulation has its origins in the inner region of the plasma disk, most likely from a centrifugally driven convective instability and an associated plasma outflow that slowly slips in phase relative to Saturn's internal rotation. The slippage rate is determined by the electrodynamic coupling of the plasma disk to Saturn and by the drag force exerted by its interaction with the Enceladus neutral gas torus.

Because Saturn is a giant gaseous planet, its internal rotation period cannot be accurately determined from visual observations. Although it has been long accepted that the magnetic dipole axis of Saturn is aligned almost exactly with its rotational axis (*1*, *2*), various magnetospheric phenomena display rotational modulation effects near its nominal rotation period (*3*–*5*). Of these, the most thoroughly studied is Saturn kilometric radiation (SKR), which is an intense radio emission discovered during the 1980–1981 Voyager flybys of Saturn (*3*). The SKR modulation period was determined by Voyager to be 10 hours, 39 min, 24 ± 7s (*6*). This value is now the internationally accepted rotation period of Saturn (*7*). More recently, radio measurements from the Ulysses and Cassini spacecraft (*8*–*10*) have shown that the SKR modulation period varies by as much as 1% on time scales of years. Because of its large inertia, the internal rotation period cannot possibly have changed by such a large amount. How then is the SKR period related to the rotation period of the interior of Saturn? In this paper we show that the SKR modulation is directly linked to the rotational modulation of plasma and magnetic fields in the inner region of Saturn's plasma disk, near the moon Enceladus, which orbits Saturn at 3.95 Saturn radii (R_S) (1 Saturn radius = 60,268 km). We propose that the rotational modulation is caused by a centrifugally driven two-cell convective instability in the plasma disk that originates from its interaction with the neutral gas torus produced by Enceladus. This instability causes a rotating plasma outflow that imposes rotational control on other processes farther out in the magnetosphere, such as the generation of SKR.

Saturn's plasma disk, sometimes also called the plasma sheet or plasmasphere, is a dense corotating plasma with a north-south thickness of about 1 to 2 R_S that extends outward into the magnetosphere from near the outer edge of the A ring (*11*, *12*). The co-rotation is caused by electromagnetic forces imposed by currents that flow along the highly conducting magnetic field lines between the plasma disk and the upper atmosphere of Saturn. Most of the plasma in the plasma disk is believed to originate from ionization of a torus of neutral gas that is present near the orbit of Enceladus. This torus originates from geyserlike plumes of water on Enceladus that inject water vapor and ice particles into orbit around Saturn (*13*–*15*). Because of the rapid rotation of the plasma disk, the centrifugal force at these radial distances is substantially larger than Saturn's gravitational force. Interchange motions driven by the centrifugal force then act to transport the plasma outward into the magnetosphere. Because the plasma particles are constrained by electromagnetic forces to move approximately along magnetic field lines, the centrifugal force also acts to concentrate the plasma near the equatorial plane, thereby forming the disklike structure.

The data used in this study are from the Radio and Plasma Wave Science (RPWS) and Magnetometer (MAG) instruments on the Cassini spacecraft, which is in orbit around Saturn. In an earlier study (*16*) using electron density measurements from the RPWS, we noticed that in the vicinity of Enceladus' orbit, from about 3 to 5 R_S, the electron density is often quite different on the inbound and outbound portions of the same pass (Fig. 1). This variability was initially thought to be attributable to the spacecraft position relative to Enceladus, but further study showed that it was not so. Instead, using the time-variable SKR longitude system introduced by Kurth *et al*. (*17*), we found (Fig. 2) that the electron density in the inner region of the plasma disk has a nearly sinusoidal variation with SKR longitude and that this variation is in phase with a similar nearly sinusoidal variation in the azimuthal, B_φ, component of the magnetic field in the plasma disk. This relation strongly suggests that the plasma density and magnetic field in the inner region of the plasma disk have a rotational control that is directly linked to the time-variable period of the SKR modulation.

By itself, a sinusoidal longitude variation does not provide proof of rotational control, even though the longitude is measured relative to a rotating reference. To demonstrate rotational control, it is essential that measurements be made over a range of local times in order to confirm that the longitude is the controlling variable. Fortunately, the orbit of Cassini provides good local-time coverage and longitude coverage of both the magnetic field and the electron density (figs. S1 and S2). A simple test can then be performed to confirm rotational control. This test consists of plotting the measured quantities as a function of the longitude relative to some fixed direction, such as the Sun. This test shows that the amplitude of the modulation decreases and the spread of the data points relative to the best fit increases significantly (compare Fig. 2, B and C, with fig. S4, B and C), thereby providing convincing evidence that both the magnetic field and the

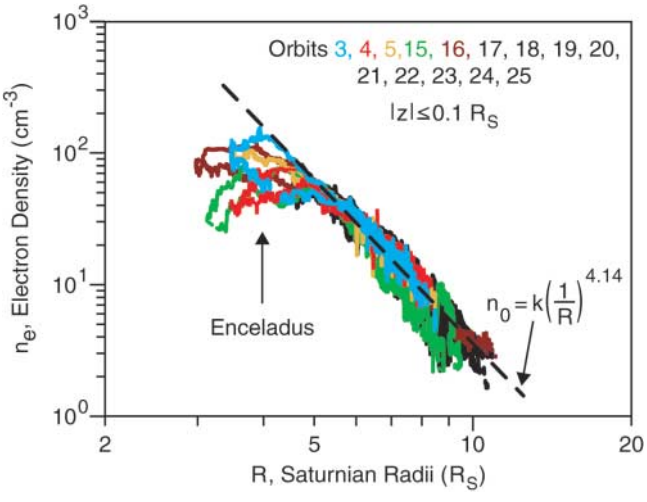

Fig. 1. The electron density n_e obtained from Cassini RPWS upper hybrid resonance measurements (*20*) for 14 equatorial orbits from 1 July 2004 to 1 July 2006. The dashed line is a power-law fit to the region beyond 5 R_S, and $k = 5.5 \times 10^4$ cm^{-3} $R_S^{4.14}$ is the constant in the power law. Only equatorial orbits with a north-south distance z from the equatorial plane less than 0.1 R_S were used in this study. There are large variations from the power-law fit in the region from 3 to 5 R_S. By following the colored line for a given orbit, one can see that the electron densities for the inbound and outbound portions of the same pass are often quite different. This hysteresis-like dependence on radial distance strongly suggests a longitudinal control.

[1]Department of Physics and Astronomy, University of Iowa, Iowa City, IA 52242, USA. [2]Blackett Laboratory, Imperial College, London SW7 2AZ, UK. [3]European Space Agency, 75738 Paris, France.

plasma density in the inner region of the plasma disk rotate at a rate that is synchronous with the time-variable SKR modulation. For other factors that could affect this interpretation, such as aliasing due to data gaps, and for an analysis of the slow long-term time variations in the rotation rate, see the supporting online material (SOM).

The occurrence of a large rotational modulation of the plasma and magnetic fields deep in the inner region of the magnetosphere that is phase-locked to the time-variable SKR modulation is surprising. Most of the rotational effects that have previously been reported occur much farther out in the magnetosphere. That the density modulation occurs near the orbit of Enceladus strongly suggests that the rotational effects observed farther out in the magnetosphere are driven by some rotational process that involves an interaction with the Enceladus neutral gas torus. This conclusion is consistent with the view that the general direction of energy flow should be outward, away from the source of the plasma and in the direction of the centrifugal force. In fact, this direction for the propagation of rotational disturbances has already been suggested and is the basis for the "camshaft" model proposed by Espinosa *et al*. (*4*). In this model, an unspecified rotating disturbance, the "cam," as in the camshaft of an engine, produces plasma and magnetic field disturbances that propagate outward into the magnetosphere. Here we propose that the newly discovered rotational density modulation in the inner region of the plasma disk acts as the cam that drives other rotationally modulated effects farther out in the magnetosphere. The main questions that remain are how are these rotational effects produced in the inner region of the magnetosphere, and how does the rotation rate relate to the internal rotation of Saturn?

Because there is presently no accepted mechanism for imposing a time-variable rotation rate from a source internal to Saturn, we proceed by exploring the possibility that the time variability arises entirely within the plasma disk. It is already widely accepted (*18*, *19*) that the rotation of the plasma disk is due to forces produced by field-aligned currents that link the plasma disk to Saturn (Fig. 3A). A very natural explanation for the time-variable rotation rate is then that the plasma disk slips at a time-variable rate relative to the upper atmosphere of Saturn, which is where the coupling to the planet takes place. The mechanism for driving this slippage could then be ionization and charge exchange in the neutral gas torus, both of which produce a drag force that opposes the rotation of the plasma disk. This process is called mass loading (*19*). In this model, the slippage rate is determined by the rate dm/dt (m, mass; t, time) at which mass is picked up by the plasma disk, and by the conductivity of the upper atmosphere, which controls the field-aligned currents that link the plasma disk to the planet. Because the ejection of mass from Enceladus probably has long-term variations that affect the density of the neutral gas torus, this model provides a ready explanation for the somewhat irregular long-term variations in the SKR modulation period (*9*). It is already known that the Enceladus neutral gas torus has variations on time scales of months (*20*), so variations on much longer time scales are highly likely. Another possible long-term effect that could cause changes in the rotation rate of the plasma disk is the seasonal variation of the solar inclination angle, which affects the conductivity of the upper atmosphere and thereby the coupling to the planet.

To proceed further, we must next explain how the density modulation is produced in the inner region of the plasma disk. A possible model is motivated by the two-cell convection mechanism suggested by Dessler *et al*. (*21*), which was originally proposed to explain rotational effects in the magnetosphere of Jupiter and was also suggested to apply to Saturn by Hill *et al*. (*22*). In our adaptation of this model (Fig. 3B), the two-cell convection pattern has its origin as a centrifugally driven instability in the plasma disk (*23*) near the orbit of Enceladus. Such convective instabilities are well known in laboratory plasma machines. As the plasma flows around the convection cycle (indicated by the closed streamlines in Fig. 3B), it picks up newly ionized plasma as it passes through the neutral gas torus (along the path from a to b in Fig. 3B), thereby increasing the plasma density. It is this density increase that accounts for the longitudinal density variations observed in the inner region of the plasma disk. The density increase also ensures that the centrifugal force, $F_c = nm\omega^2 R$, where n is the plasma number density, m is the molecular mass, ω is the rotation rate, and R is the radial distance, at point $F_c(2)$ is higher than at a symmetrically located point $F_c(1)$. It is this difference in the centrifugal forces that drives the convection. From the ionization rate given by Hansen *et al*. (*24*) for the neutral gas torus, 8.7×10^{-5} cm^{-3} s^{-1}, we estimate that it takes about a week to produce the observed ~50 cm^{-3} peak-to-peak density variation as the plasma flows through the neutral gas torus.

Most previous models of centrifugally driven convection suggest that the convective motions should be dominated by high-order, $m >> 1$, azimuthal modes that evolve into fingerlike azimuthal structures (*25*, *26*). However, these models do not consider the process by which the plasma is produced. For an azimuthally symmetric plasma source, such as the Enceladus neutral gas torus, we believe that the lowest-order m = 1 (two-cell) mode should dominate, because this mode produces the longest path length through the source region, thereby giving the largest density increase and the largest growth rate for the instability. Because there is a continuous production of plasma from the torus, in a steady state there must be a corresponding outflow of plasma from the plasma disk into the outer re-

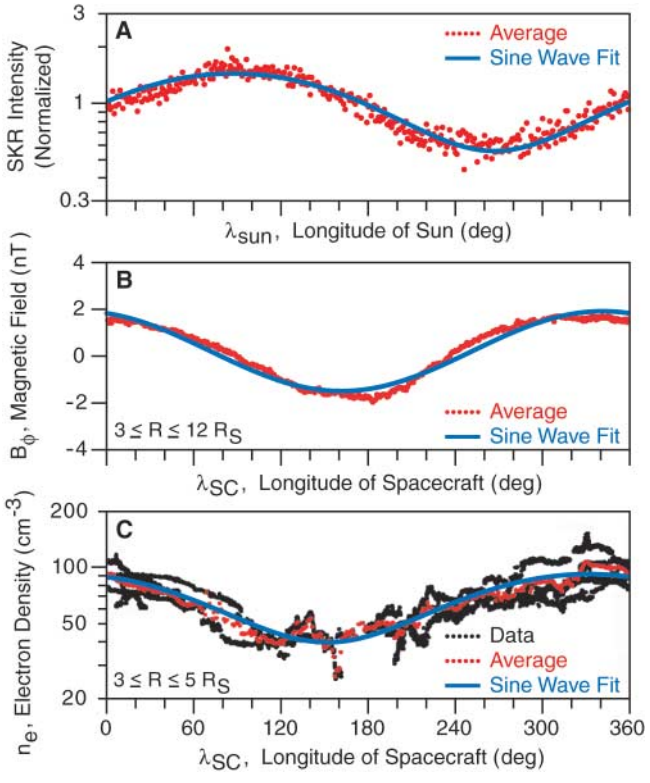

Fig. 2. (**A**) The normalized SKR intensity as a function of the longitude of the Sun, λ_{Sun}, using the time-variable SKR longitude system introduced by Kurth *et al*. (*17*). The longitude of the Sun is used in this plot because the SKR modulation is known to be a purely temporal variation (*29*), like a flashing light, not a rotating beacon. The characteristic nearly sinusoidal modulation of the SKR intensity is clearly apparent. (**B**) The average azimuthal B_ϕ component of the magnetic field in the plasma disk (3 to 12 R_S) as a function of the SKR longitude of the spacecraft λ_{SC}. λ_{SC} is used because we anticipated that the magnetic field would have a rotational control, as has been assumed by other authors (*4*). As can be seen, the magnetic field displays a very clear, nearly sinusoidal dependence on λ_{SC}. (**C**) The electron density as a function of λ_{SC}, where again we anticipated a possible rotational control. The radial distance range in this case has been limited to the inner region of the plasma disk (3 to 5 R_S), because this is the region where the electron density variations are the largest (Fig. 1). A very clear, nearly sinusoidal modulation is evident, with an amplitude variation of nearly a factor of 2 and a phase at the peak (λ_{SC} ~ 330°) that is almost the same as for the magnetic field.

gions of the magnetosphere. The two-cell convection would then cause a concentration of the outflowing plasma on the dense side of the convection pattern (Fig. 3B); that is, at an SKR longitude of $\lambda_{SC} \sim 330°$. As the convection pattern rotates, this outflow would produce perturbations that propagate far out into the magnetosphere, thereby acting as the cam that drives other rotationally modulated magnetospheric effects, such as the SKR. From the Voyager 1 and 2 radio observations (*27*), it is known that SKR is generated at relatively low altitudes along magnetic field lines that pass near the magnetopause on the late-morning side of the magnetosphere. As the perturbations from $\lambda_{SC} \sim 330°$ propagate outward, the associated magnetic field perturbations (fig. S3) develop a phase lag of about 149° to 195° by the time they reach the vicinity of the magnetopause at $R \sim 20\ R_S$. This phase lag, which has been previously studied by Espinosa *et al*. (*4*) and Cowley *et al*. (*28*), is almost exactly the right amount to explain the generation of SKR in the late morning at a local time of about 8 to 11 hours and a subsolar SKR longitude of $\lambda_{Sun} = 100°$. For a further discussion of the geometry involved and for comments on how the SKR might be generated as the outward-propagating disturbance from the cam interacts with the morning side of the magnetopause, see the SOM.

A potentially important feature of the convection pattern that needs to be explained is the close relation between the phase of the azimuthal magnetic field and the phase of plasma density modulation (Fig. 2, B and C). This relation is most likely related to the azimuthal torque required to oppose the change in the angular momentum of the plasma disk caused by the mass loading. Because both ionization and charge exchange are proportional to the plasma density, they both contribute to the mass loading. The current system that produces this torque and the resulting contribution to the B_φ magnetic field are then expected to be largest in the region of highest plasma density, which would explain why these two quantities are in phase. However, the relation between the magnetic field and the plasma density variations may be more subtle. If the current systems linking the plasma sheet to the northern and southern hemispheres are identical, then there would be no B_φ magnetic field component at the equator. The equatorial B_φ component would then have to be due to an asymmetry between northern and southern hemispheres. The asymmetry could be produced by the fact that the net dayside conductivity of the southern hemisphere of Saturn is currently higher than in the northern hemisphere, not only because high southerly latitudes are currently in sunlight but also because the rings are partially shadowing the northern hemisphere. This north-south difference in the illumination greatly increases the conductivity of the upper atmosphere in the southern hemisphere relative to that in the northern hemisphere. The immediate consequence of this difference is that interchange motion would be resisted more by the southern ionosphere (*23*). In the high-density sector where flux tubes would move out, the northern ionosphere has to transmit a poleward motion to the southern ionosphere and vice versa in the inward-moving sector. This asymmetry would require a significant transverse magnetic field component at the equator. A quarter-cycle lag is expected between outward motion and the peak bending inward of the field (that is, a peak negative value of the radial field perturbation, ΔB_r). Recalling the phase relation originally identified by Espinosa *et al*. (*4*) (that ΔB_r leads B_φ), one sees that the observed phase relation between B_φ and n_e (n_e, electron density) is consistent.

Because our model is based on a centrifugally driven instability in the plasma disk that acts as a camshaft, it does not necessarily require a rotating magnetic anomaly or any other rotating source internal to Saturn. Therefore, the internal rotation period of Saturn cannot be determined from the period of the SKR modulation. The only conclusion that can be drawn is that the internal rotation period must be less than the shortest SKR modulation period ever observed, which currently is slightly less than the period observed by Voyager (*9*). If some internal source with the correct time-variable rotation rate were to be eventually identified, it is clear that any new explanation would need to account for the rotating plasma density and magnetic fields reported in this paper, as well as their linkage to the time-variable SKR modulation rate.

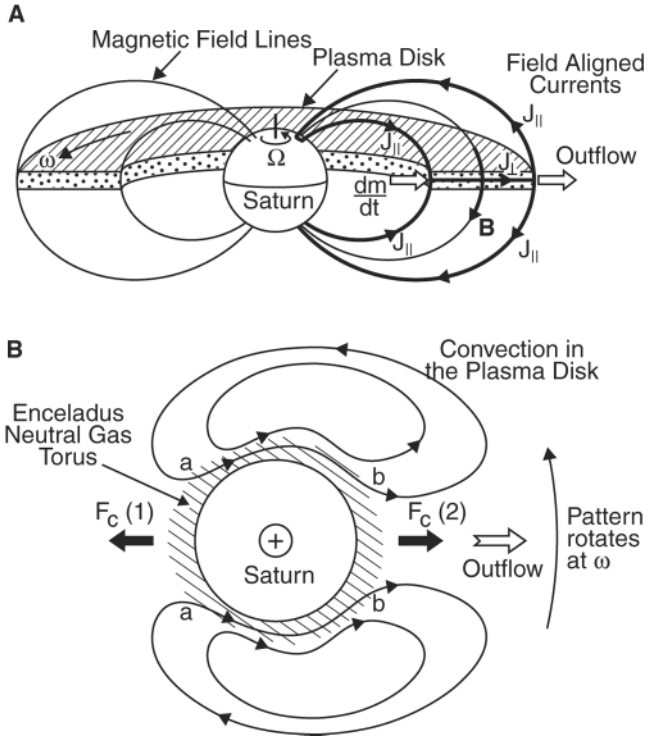

Fig. 3. (**A**), adapted from Hill (*18*), shows the mechanism by which the plasma disk is coupled to the upper atmosphere of Saturn via magnetic field–aligned currents, $\mathbf{J}_\parallel$. The field-aligned currents transfer angular momentum from the planet to the plasma disk via the $\mathbf{J}_\perp \times \mathbf{B}$ force exerted, where $\mathbf{J}_\perp$ is the component of current flowing perpendicular to the magnetic field **B**. This force opposes the drag force exerted on the disk as mass produced by ionization and charge exchange from the Enceladus gas torus is picked up by the rapidly rotating magnetic field. This drag force causes the plasma disk, which rotates at an angular rate ω, to slip slowly with respect to the rotation rate Ω of the upper atmosphere of Saturn. (**B**) The rotating two-cell plasma convection pattern that we propose to explain the longitudinal modulation of the plasma density and magnetic field in the inner region of the plasma disk. In this model, the two-cell convection pattern, shown as viewed from the north pole of Saturn, is driven by a centrifugal instability that arises from ionization of the neutral gas torus. As the plasma flows through the neutral gas torus from a to b, the density increases because of this ionization, causing the centrifugal force $F_c = nm\omega^2 R$ at $F_c(2)$ to be greater than at the symmetrical point $F_c(1)$ on the opposite side of the convection pattern. It is this difference in the centrifugal forces that drives the convection. A radial outflow of plasma in the "heavy" sector of the convection pattern then acts as the cam (*4*) that drives the rotational modulation of various phenomena in the outer magnetosphere, such as the SKR. The slippage rate, and therefore the SKR modulation period, are determined by the mass loading rate *dm*/*dt* from the neutral gas torus and by the coupling to the upper atmosphere, both of which are likely to have long-term variations.

References and Notes

1. E. J. Smith *et al.*, *Science* **207**, 407 (1980).
2. J. E. P. Connerney, L. Davis Jr., D. L. Chenette, in *Saturn*, T. Gehrels, M. S. Matthews, Eds. (Univ. of Arizona Press, Tucson, AZ, 1984), pp. 354–377.
3. J. W. Warwick *et al.*, *Science* **212**, 239 (1981).
4. S. A. Espinosa, D. J. Southwood, M. K. Dougherty, *J. Geophys. Res.* **108**, 1086 (2003).
5. G. Giampieri, M. K. Dougherty, E. J. Smith, C. T. Russell, *Nature* **441**, 62 (2006).
6. M. D. Desch, M. L. Kaiser, *Geophys. Res. Lett.* **8**, 253 (1981).
7. M. E. Davies *et al.*, *Cel. Mech. Dyn. Astron.* **63**, 127 (1996).
8. A. Lecacheux, P. Galopeau, M. Aubier, *Planetary Radio Emissions IV*, H. O. Rucker, S. J. Bauer, A. Lecacheux, Eds. (Austrian Academy of Sciences Press, Vienna, 1997).
9. P. H. M. Galopeau, A. Lecacheux, *J. Geophys. Res.* **105**, 13089 (2000).
10. D. A. Gurnett *et al.*, *Science* **307**, 1255 (2005).
11. D. T. Young *et al.*, *Science* **307**, 1262 (2005).
12. H. S. Bridge *et al.*, *Science* **212**, 217 (1981).
13. C. C. Porco *et al.*, *Science* **311**, 1393 (2006).
14. M. K. Dougherty *et al.*, *Science* **311**, 1406 (2006).
15. J. H. Waite Jr. *et al.*, *Science* **311**, 1419 (2006).

16. A. M. Persoon *et al.*, *Geophys. Res. Lett.* **32**, L23105 (2005).
17. W. S. Kurth, A. Lecacheux, T. F. Averkamp, J. B. Groene, D. A. Gurnett, *Geophys. Res. Lett.* **34**, L02201 (2007).
18. T. W. Hill, *J. Geophys. Res.* **84**, 6554 (1979).
19. A. Eviatar, R. L. McNutt Jr., G. L. Siscoe, J. D. Sullivan, *J. Geophys. Res.* **88**, 823 (1983).
20. L. W. Esposito *et al.*, *Science* **307**, 1251 (2005).
21. A. J. Dessler, R. R. Sandel, S. K. Atreya, *Planet. Space Sci.* **29**, 215 (1981).
22. T. W. Hill, A. J. Dessler, L. J. Maher, *J. Geophys. Res.* **86**, 9020 (1981).
23. D. J. Southwood, M. G. Kivelson, *J. Geophys. Res.* **94**, 299 (1989).
24. K. C. Hansen *et al.*, *Geophys. Res. Lett.* **32**, L20S06 (2005).
25. G. L. Siscoe, D. Summers, *J. Geophys. Res.* **86**, 8471 (1981).
26. Y. S. Yang, R. A. Wolf, R. W. Spiro, T. W. Hill, A. J. Dessler, *J. Geophys. Res.* **99**, 8755 (1994).
27. P. Zarka, *J. Geophys. Res.* **103**, 20, 159–20, 194 (1998).
28. S. W. H. Cowley *et al.*, *Geophys. Res. Lett.* **33**, L07104 (2006).
29. M. L. Kaiser *et al.*, in *Saturn*, T. Gehrels, M. S. Matthews, Eds. (Univ. of Arizona Press, Tucson, AZ, 1984), pp. 378–415.

30. The research at the University of Iowa was supported by NASA through contract 1279973 with the Jet Propulsion Laboratory.

Supporting Online Material

www.sciencemag.org/cgi/content/full/1138562/DC1
SOM Text
Figs. S1 to S8
References

7 December 2006; accepted 7 March 2007
Published online 22 March 2007;
10.1126/science.1138562
Include this information when citing this paper.

www.sciencemag.org/cgi/content/full/1138562/DC1

Supporting Online Material for

The Variable Rotation Period of the Inner Region of Saturn's Plasma Disk

D. A. Gurnett, A. M. Persoon, W. S. Kurth, J. B. Groene, T. F. Averkamp, M. K. Dougherty, D. J. Southwood

Published 22 March 2007 on *Science* Express
DOI: 10.1126/science.1138562

This PDF file includes:

Supporting Online Material

The Variable Rotation Period of the Inner Region of Saturn's Plasma Disk

D. A. Gurnett,[1*] A. M. Persoon,[1] W. S. Kurth,[1] J. B. Groene,[1]
T. F. Averkamp,[1] M. K. Dougherty,[2] D. J. Southwood[2,3]

[1]Department of Physics and Astronomy, University of Iowa, Iowa 52242, USA.
[2]Blackett Laboratory, Imperial College, London SW72AZ, UK.
[3]European Space Agency, 75738 Paris, France.
*To whom correspondence should be addressed. E-mail: donald-gurnett@uiowa.edu

Data

The data used in this paper are from the Radio and Plasma Wave Science (RPWS) and Magnetometer (MAG) instruments on the Cassini spacecraft (*S1, S2, S3*), which was placed in orbit around Saturn on July 1, 2004. The measurements of the intensity of the Saturn kilometric radiation (SKR) are obtained from the RPWS electric field antennas. To provide a measurement of the broadband SKR intensity, the electric field spectral densities have been integrated from 20 kHz to 500 kHz and averaged over time intervals of 10 minutes. These broadband intensities are then divided by four-rotation averages in order to obtain a normalized intensity that corrects to first-order for the radial distance dependence. The local electron density is obtained from the RPWS by measuring of the frequency of electostatic plasma oscillations at the upper hybrid resonance (UHR) frequency. The UHR frequency is given by $f_{UHR} = \sqrt{f_c^2 + f_p^2}$, where f_c is the electron cyclotron frequency and f_p is the electron plasma frequency. The electron cyclotron frequency is given by $f_c = 28B$ Hz, where B is the magnetic field strength in nT, and the electron plasma frequency is given by $f_p = 8980\sqrt{n_e}$ Hz, where n_e is the electron number density in cm^{-3}. For further details on the derivation of these equations, see Gurnett and Bhattacharjee (*S4*). Using the above equations it is easy to show that the electron density is given by $n_e = (f_{UHR}^2 - f_c^2)/(8980)^2$ cm^{-3}. Since the wavelengths of the upper hybrid waves are generally much larger than the dimensions of the plasma sheath that surrounds the spacecraft, the upper hybrid technique has the advantage that the density measurements are not influenced by spacecraft charging or other effects that typically affect other types of measurements of the local plasma density. When the upper hybrid emission is strong and well-defined the electron density can usually be determined to an accuracy of about ±10%. For a further discussion of the upper hybrid resonance technique for measuring electron densities, see Persoon *et al.* (*S5*). For the magnetic field data the three magnetic field components measured in the spacecraft (x, y, z) coordinate system are converted to a right-handed (r, θ, φ) coordinate system, where r is the radial

component measured positive outward from the center of the planet, θ is the polar angle measured positive southward from the north pole, and φ is measured positive in the sense of the planetary rotation.

Orbital Coverage

To properly assess the quality of these results, it is important to understand the degree to which the orbit of Cassini provides samples of key variables. To simplify the analysis, the orbits analyzed have been restricted to those within a north-south distance of $z = \pm 0.1\ R_S$ of the equatorial plane, thereby eliminating latitude as a variable. These are orbits 3, 4, and 5, and orbits 15 through 25. Three variables then remain that are of potential interest: (1) the radial distance R from the center of the planet; (2) the local time LT, which is the hour angle measured counter-clockwise in the equatorial plane from local midnight; and (3) the spacecraft SKR longitude, λ_{SC}, which is measured positive westward (clockwise as viewed from the north pole) from the reference longitude defined by Kurth *et al.* (*S6*). The degree to which these variables have been sampled can be represented by the two polar plots shown in Figs. S1 and S2. The first plot (Fig. S1) shows that in the radial distance range from 3 to 12 R_S, which is primarily important for the magnetic field analysis, the local time coverage has a substantial gap in the afternoon sector at large radial distances, from about 12 to 18 hours LT. A somewhat smaller gap exists at all radial distances from about 4 to 6 hours LT. Since the phase and amplitude of the B_φ magnetic field is very nearly constant over the range from 3 to 12 R_S (Fig. S3), and since the B_φ magnetic field data were averaged over this entire range, these gaps have very little effect on the magnetic field analysis. However, in the region where the large electron density variations occur, from 3 to 5 R_S, the local time coverage is not as good. There is no data in this region for local times from about 1 hour to 13 hours LT. The possible implications of this data gap on the analysis of the electron density are discussed in the following two sections. The second plot (Fig. S2) shows that the coverage of SKR longitude is very good at all radial distances. This good coverage mainly arises because of the rapid rotation of the SKR longitude system, which allows the spacecraft to cover a very wide range of longitudes on any given pass, even inside of 5 R_S.

Test of Rotational Control

The magnetic field and electron density plots in Figs. 2B and 2C show a very clear nearly sinusoidal dependence on the SKR longitude of the spacecraft. However, before we can claim that this longitude dependence is due to rotational control, we must perform the following simple test. If the data are plotted in a non-rotating frame of reference, such as with respect to the Sun, then the modulation amplitudes must decrease, and the spread in the data points relative to the best-fit must increase. The results of this test are shown in Fig. S4, which is similar to Fig. 2, but with the longitude of the spacecraft, λ_{SC}, replaced by the longitude of the Sun, λ_{Sun}. As can be seen, the amplitude of the magnetic field modulation in Fig. S4B has decreased markedly compared to the corresponding amplitude in Fig. 2B. That the decrease in the modulation amplitude is consistent with what is to be expected from the available local time coverage is

demonstrated in Fig. S5B. This illustration uses the best-fit sine wave (blue line) in Fig. 2B as "simulated data," and shows a plot of the simulated data as a function of the longitude of the Sun using the same spacecraft trajectory as for the "real" data. A comparison of Figs. S4B and S5B clearly shows that the decrease in the modulation amplitude is consistent with what would be expected for rotational control. A similar set of plots, Figs. S4C and S5C, has been constructed to test the electron density for rotational control. Fig. S4C clearly shows a decrease in the modulation amplitude and a marked increase in the spread of the data points compared to Fig. 2C, again consistent with rotational control. However, the changes are not as dramatic as for the magnetic field, because the local time coverage in the region where the electron density has been sampled, 3 to 5 R_S, is not nearly as complete as for the magnetic field, see Fig. S1. To see if the observed reduction in the modulation amplitude and the increased spread in the data points are consistent with the changes expected for the available local time coverage, Fig. S5C has been constructed using the same "simulated data" technique that was used for the magnetic field data. A comparison of Figs. S4C and S5C clearly shows that the observed changes in the modulation amplitude and the spread in data are consistent with what is to be expected given the available local time coverage.

We have also considered the possibility that if the electron density were to have a strong radial gradient in the region from 3 to 5 R_S, then there might be some longitudinally dependent correlation with the radial distance that would appear as an apparent rotational modulation. However, we believe that this is not likely, since the average electron density profile given by Persoon *et al.* (*S5*) shows only a very small radial gradient in the region from 3 to 5 R_S, certainly much smaller than the observed variations. Also, the orbital trajectories (Fig. S2) show no obvious correlation between radial distance and longitude in the region from 3 to 5 R_S.

Aliasing and the Effect of Variations in the Rotation Rate

In addition to the evidence of rotational control described in the text, it is worth considering various other complications that can arise in this type of analysis. One such complication is that there are gaps in both the plasma density and magnetic field data. These gaps arise because of the highly eccentric orbit of Cassini, which only allows measurements to be made in the inner region of the magnetosphere during periapsis passes. Typically, only one such pass occurs every few weeks. Because of these gaps false periodicities can easily arise, an effect called aliasing. Fortunately, the SKR measurements do not tend to suffer from this problem since the SKR intensities are measured nearly continuously, independent of the spacecraft position. To test the robustness of our results, we carried out a parametric analysis of the various factors involved in the SKR longitude computation. As described by Kurth *et al.* (*S6*), the SKR longitude is computed by introducing a phase correction, $\varphi(T)$, to an assumed constant rotation rate Ω_0, where $T = t - t_0 - R(t)/c$ is the time relative to some epoch t_0, corrected for the light travel time $R(t)/c$. The phase correction is taken to be a third-order polynomial of the form $\varphi(T) = C_1 + C_2T + C_3T^2 + C_4T^3$. The constants C_0, C_1, C_2, C_3, and C_4 have been determined from a best-fit to the SKR intensity variations and are given by Kurth *et al.* (*S6*) for an epoch time of t_0 = January 1, 2004. For our purposes we have concentrated our analysis on the instantaneous rotation rate, $\omega = d\lambda_{Sun}/dt$, which from the

definition $\lambda_{Sun} = C_0 + \Omega_0 T - \varphi(T)$ given by Kurth *et al.* (*S6*) is easily shown to be $\omega = \Omega_0 - C_2 - 2C_3 T - 3C_4 T^2$, where we have omitted the relatively minor light travel time correction. This equation can be viewed as a truncated Taylor series expansion of the form

$$\omega = \omega_0 + \frac{\partial \omega}{\partial T}\left(T - T_0\right) + \frac{1}{2}\frac{\partial^2 \omega}{\partial T^2}\left(T - T_0\right)^2, \qquad \text{(S1)}$$

where T_0 is the time around which the expansion is computed, and ω_0, $\partial\omega/\partial t$, and $(1/2)\partial^2\omega/\partial T^2$ are the expansion coefficients evaluated at time T_0. The meaning of these various terms is illustrated in Fig. S6. It is easily shown that the coefficients in the Taylor series expansion are linked to the C_n constants via a system of linear equations. Specifically, $\omega_0 = \Omega_0 - [C_2 + 2C_3(\Delta T_0) + 3C_4(\Delta T_0)^2]$, $\partial\omega/\partial T = -2[C_3 + 3C_4(\Delta T_0)]$, and $(1/2)\partial^2\omega/\partial T^2 = -3\ C_4$, where $\Delta T_0 = T_0 - t_0$ is the time difference relative to the epoch used by Kurth *et al.* (*S6*). It is a simple matter to invert this system of equations to obtain the C_n coefficients as a function of the expansion coefficients ω_0, $\partial\omega/\partial t$, and $(1/2)\partial^2\omega/\partial T^2$, which from now on will be considered variables. By choosing an expansion time near the center of the data analysis interval, the interdependences of the even and odd terms in the expansion can be minimized, thereby simplifying the analysis. For the time interval used in our data analysis, from T_{start} = July 1, 2004 to T_{stop} = July 1, 2006, it was convenient to choose $T_0 = (1/2)(T_{start} + T_{stop})$ = July 1, 2005 as the expansion time.

To search for possible aliasing effects, we computed the amplitudes of the best-fit sine wave to the longitude dependence of the SKR intensity, the magnetic field B_φ, and the electron density n_e, averaged over the same radial distances used in Fig. 2. We then explored the sensitivity of the amplitude of the best-fit sine wave to the expansion coefficients, ω_0, $\partial\omega/\partial t$, and $(1/2)\partial^2\omega/\partial T^2$, by varying these coefficients one at a time relative to the nominal values determined from the C_n constants used by Kurth *et al.* (*S6*). The nominal values are $\omega_0 = 800.444°/\text{day}$, $\partial\omega/\partial t = -3.4850 \times 10^{-3}\ °/\text{day}^2$, and $(1/2)\partial^2\omega/\partial T^2 = 2.3739 \times 10^{-6}\ °/\ \text{day}^3$. The variations in the amplitudes of the best-fit sine waves as a function of these parameters are shown in Fig. S7. The top row of these spectrum-like plots shows the amplitude of the SKR modulation as a function of ω_0, $\partial\omega/\partial t$, and $(1/2)\partial^2\omega/\partial T^2$. The sharp peaks in these plots are in almost exact agreement with the nominal values for these parameters from the Kurth *et al*. model, as indicated by the vertical red dashed lines. Similarly, the magnetic field modulation amplitudes in the middle row of plots are also seen to be almost exactly consistent with the nominal SKR parameters, although there is more evidence of sidebands than in the SKR plots. The sidebands are caused by the previously mentioned data gaps, which introduce extraneous periodicities in the data. Finally, the amplitude spectrums of the electron density modulation are shown in the bottom row of plots. These spectrums have considerably broader peaks and, in the case of the ω_0 plot, sidebands with substantial amplitudes. Nevertheless, the main peaks are in good agreement with the nominal SKR parameters. The electron density peaks are broader because the quantity of electron density data is much more limited than for either the magnetic field or the SKR. The strong equally spaced sidebands in the ω_0 plot arise because of a beat between two well-separated intervals where electron density data are available inside of 5 R_S, i.e., orbits 3, 4, and 5, and orbits 15, 16, 17, and 19.

Origin of the SKR Modulation

Analyses of the Voyager 1 and 2 data (*S7*, *S8*) provide strong evidence that SKR is generated by the cyclotron maser mechanism. The source is believed to be located at relatively low altitudes along high latitude magnetic field lines that pass near the magnetopause in the late local morning region of the magnetosphere. Although the precise magnetic latitude of the source is not well established, for our purposes we will assume that the magnetic field line through the source extends out to an equatorial radial distance of about R ~ 20 R_S and that the local time of the source is about LT ~ 8 to10 hr. Although the general outline of the radio emission mechanism is well known, the process that switches the radiation on once per rotation at a sub-solar longitude of λ_{Sun} ~ 100° has been somewhat of a mystery. A key to the likely explanation is given in Fig. S3, which shows the phase of the magnetic field perturbations generated by the plasma outflow as the disturbance propagates outward into the magnetosphere. This plot shows that in the inner region, from about 3 to 12 R_S, the amplitude and phase of the magnetic field perturbation remain nearly constant at λ_{SC} ~ 330°, which is where the peak in the plasma density occurs in the inner region of the plasma disk (Fig. 3C). However, beyond about 12 R_S a phase lag develops that increases linearly with increasing distance, eventually reaching a total shift of about $\Delta\lambda$ = (119° + 30°) ~ 149° to (165° + 30°) ~ 195° by the time the disturbance reaches the vicinity of the magnetopause at R ~ 20 R_S. To see if this phase lag is consistent with the generation of SKR in the late local morning region we must consider the phase relationships that exist between the SKR longitude of the outflow at λ_{SC}(outflow), the phase lag, $\Delta\lambda$, and the local time, LT, of the source. The relationship between these various quantities is illustrated in Fig. S8, which shows the geometry that exists at the time of maximum SKR intensity, i.e., λ_{Sun} = 100°. Using this diagram and the nominal values for the SKR longitude of the plasma outflow, λ_{SC}(outflow) ~ 330°, i.e., and the nominal values for the phase lag, $\Delta\lambda$ ~ 149° to 195°, gives a local time for the source magnetic field line of about LT ~ 8 to 11 hr. This local time range is in good agreement with the known source location of the SKR.

Just what turns the radio emission on as the outward propagating disturbance from the plasma outflow passes through the local time region around 8 to 10 hr is unknown, but several possibilities can be identified. First, as the rotating plasma disturbance passes near the morning side magnetosphere, the decreasing distance to the magnetopause could cause a significant compression and distortion of the magnetic field lines, particularly in the vicinity of the polar cusp, which is expected to be located at high latitudes on the dayside of the magnetosphere. These effects could produce the field-aligned currents and anisotropic distribution functions needed to drive the cyclotron maser mechanism. Second, the plasma outflow could produce an enhanced velocity shear in the region between the magnetopause and the co-rotating magnetospheric plasma. Galopeau *et al.* (*S9*) have suggested that velocity shear in this region could generate SKR by causing a Kelvin-Helmholz instability along the flanks of the magnetopause, which in turn could produce the field-aligned currents and anisotropic distribution functions needed to drive the cyclotron maser mechanism. Third, the rotating plasma disturbance associated with the outflow could cause changes in the plasma density in the SKR source region. The cyclotron maser mechanism is known to be quite sensitive to background plasma density.

Finally, we comment on the possible role that the phase lag could have on short-term variations in the period of the SKR modulation. High-time resolution studies of the SKR spectrum (*S6*) show that there are significant fluctuations in the phase of the SKR modulation at short time scales, on the order of days to weeks. Because the phase lag increases rapidly with increasing radial distance, variations in the distance to the magnetopause position, which is known to fluctuate in response to variations in solar wind pressure, would be expected to cause significant fluctuations in the phase of the SKR modulation. These phase fluctuations would appear as short-term variations in the period of the SKR modulation. Considerable further study is needed to fully understand the effects that are produced as the outward propagating disturbances from the inner region of the plasma disk interact with the magnetopause at these large radial distances.

Supporting Figures

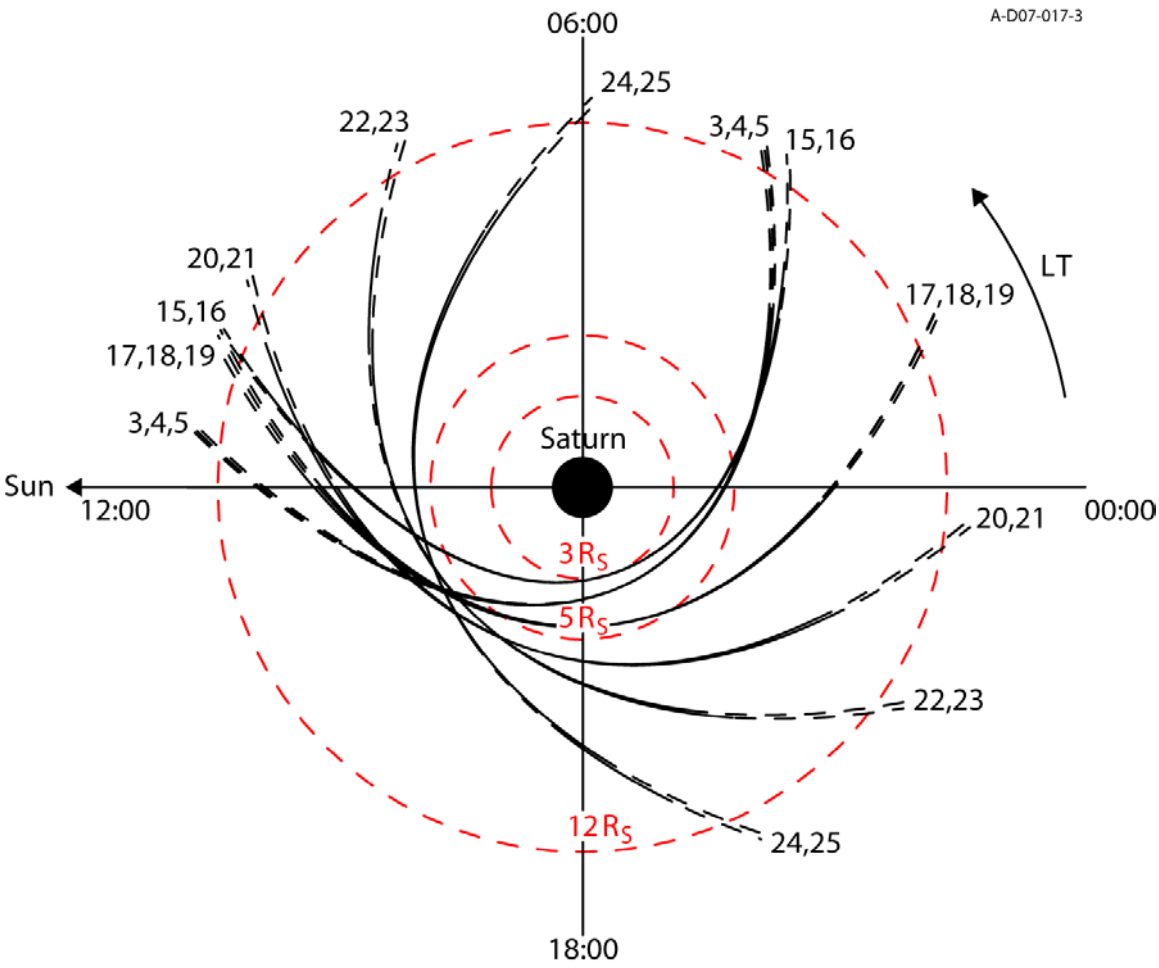

Fig. S1. This plot shows the spacecraft trajectory for all of the data analyzed as a function of radial distance and local time, LT, as viewed from the north pole with the Sun to the left. The solid lines indicate regions were both plasma density and magnetic field data are available, and the dashed lines indicate regions where only magnetic field data are available. The orbit numbers are given at the ends of the trajectories. In many cases the trajectories follow almost the same path. These coincidences arise because of constraints imposed by targeted flybys of Titan and various moons in the inner region of the Saturn system.

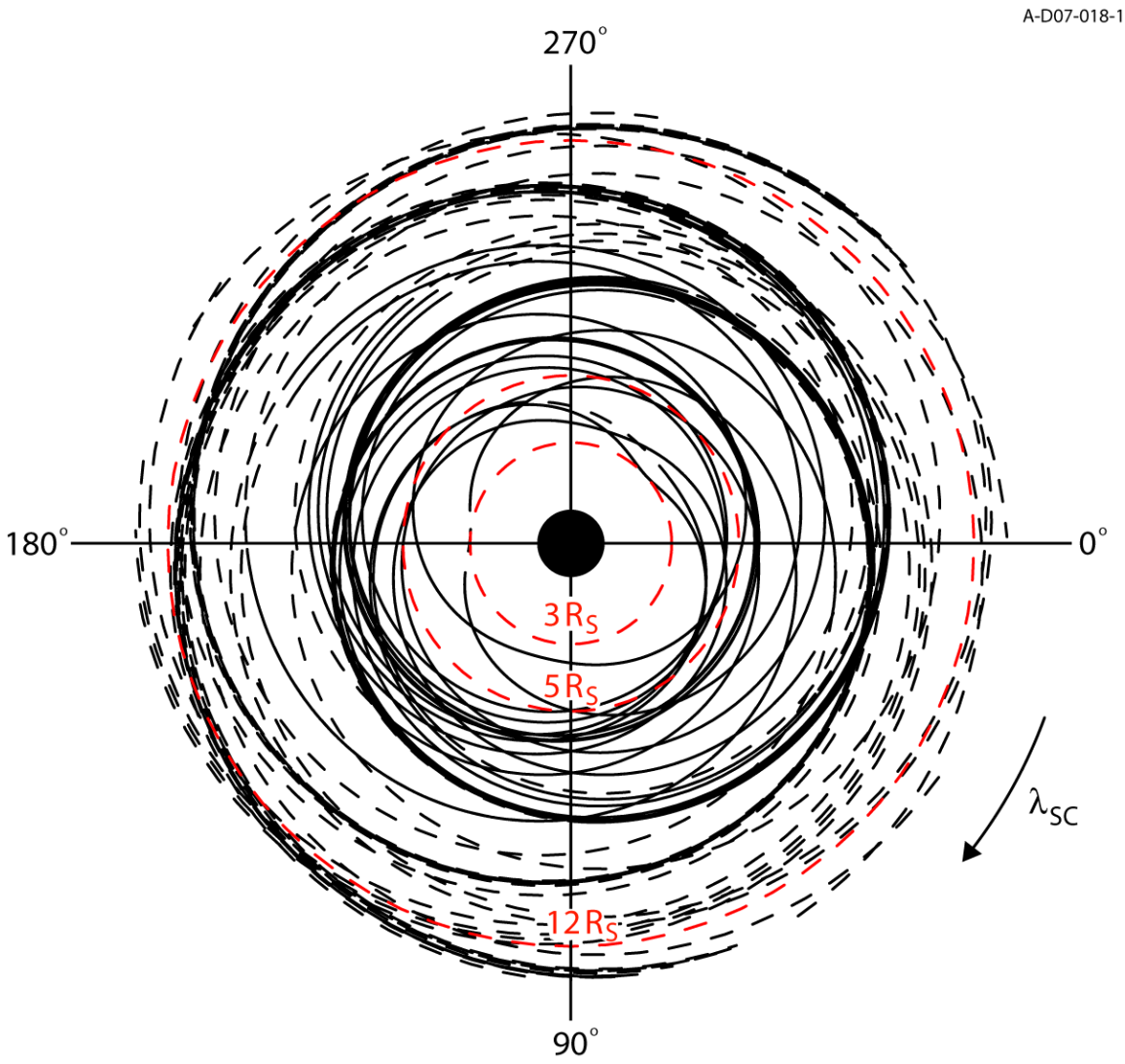

Fig. S2. This plot shows the spacecraft trajectory for all of the data analyzed as a function of radial distance and SKR longitude, as viewed looking down from the north pole with the 0° reference longitude horizontally to the right. The SKR longitude system is a west longitude system, which means that in this view the longitude is measured clockwise from the reference longitude.

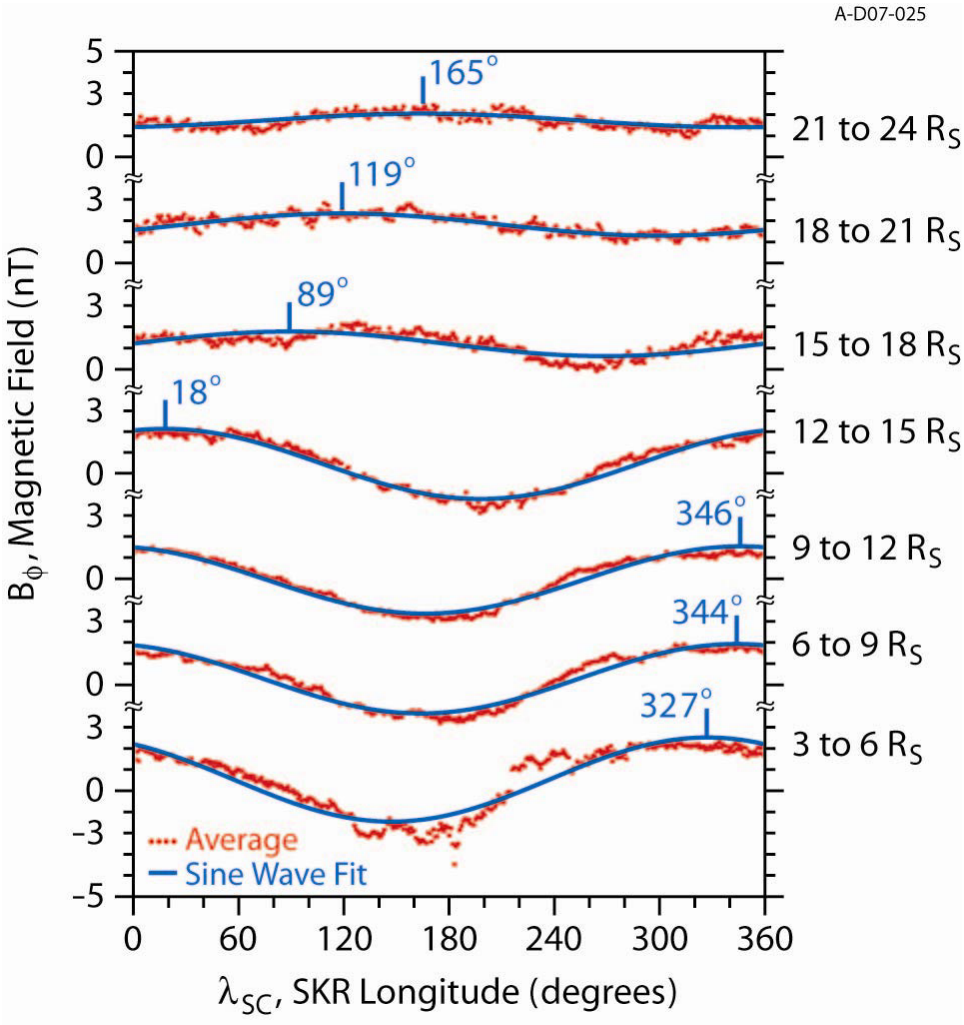

Fig. S3 A plot of B_φ versus spacecraft SKR longitude similar to Fig. 2B, but broken into eight contiguous radial distance ranges extending from 3 to 24 R_S. This plot shows that the phase and amplitude of the B_φ modulation is nearly independent of radial distance in the range from about 3 to12 R_S, but then develops a phase lag that increases linearly with increasing radial distance beyond about 12 R_S. The longitude of the peak varies from λ_{SC} ~ 330° in the inner region to approximately λ_{SC} ~ 119° to 165° by the time it reaches the vicinity of the dayside magnetopause at R ~ 20 R_S, a total phase lag of $\Delta\lambda$ ~ 149° to 195°.

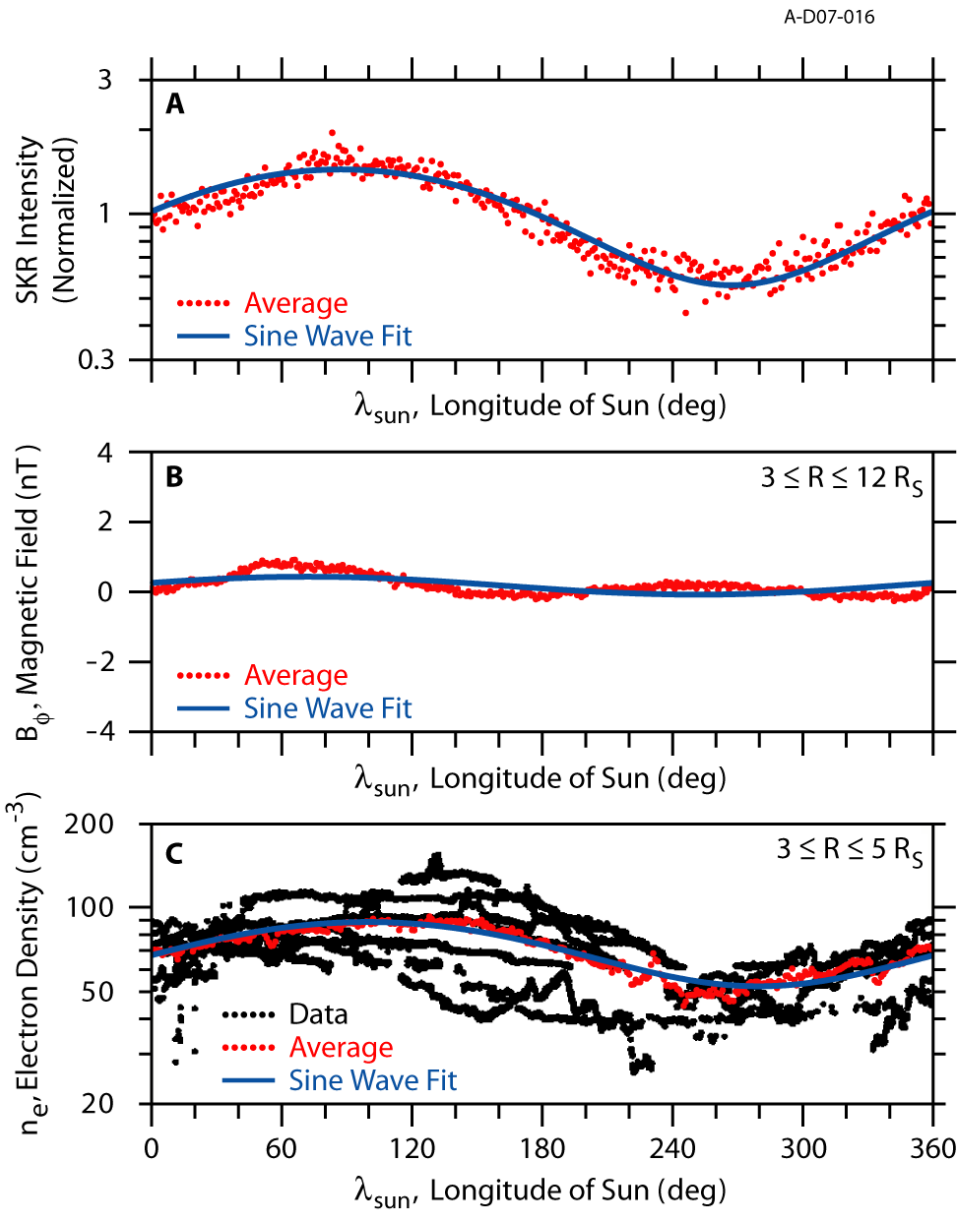

Fig. S4. This plot is like Fig. 2. However, as a test for rotational control, the B_φ magnetic field in panel (B) and the electron density in panel (C) have been plotted as a function of the SKR longitude of the Sun, λ_{Sun}, instead of the SKR longitude of the spacecraft, λ_{SC}. As can be seen, in both cases the modulation amplitudes decrease, and in the case of the electron density, the spread in the data increases compared to the corresponding plots in Fig. 2. These results are consistent with rotational control for both quantities. The relatively small change in the modulation amplitude of the electron density is due to the relatively poor local time coverage in the region from 3 to 5 R_S, as can be seen in Fig. S1. The effect of the local time coverage is explored further in Fig. S5.

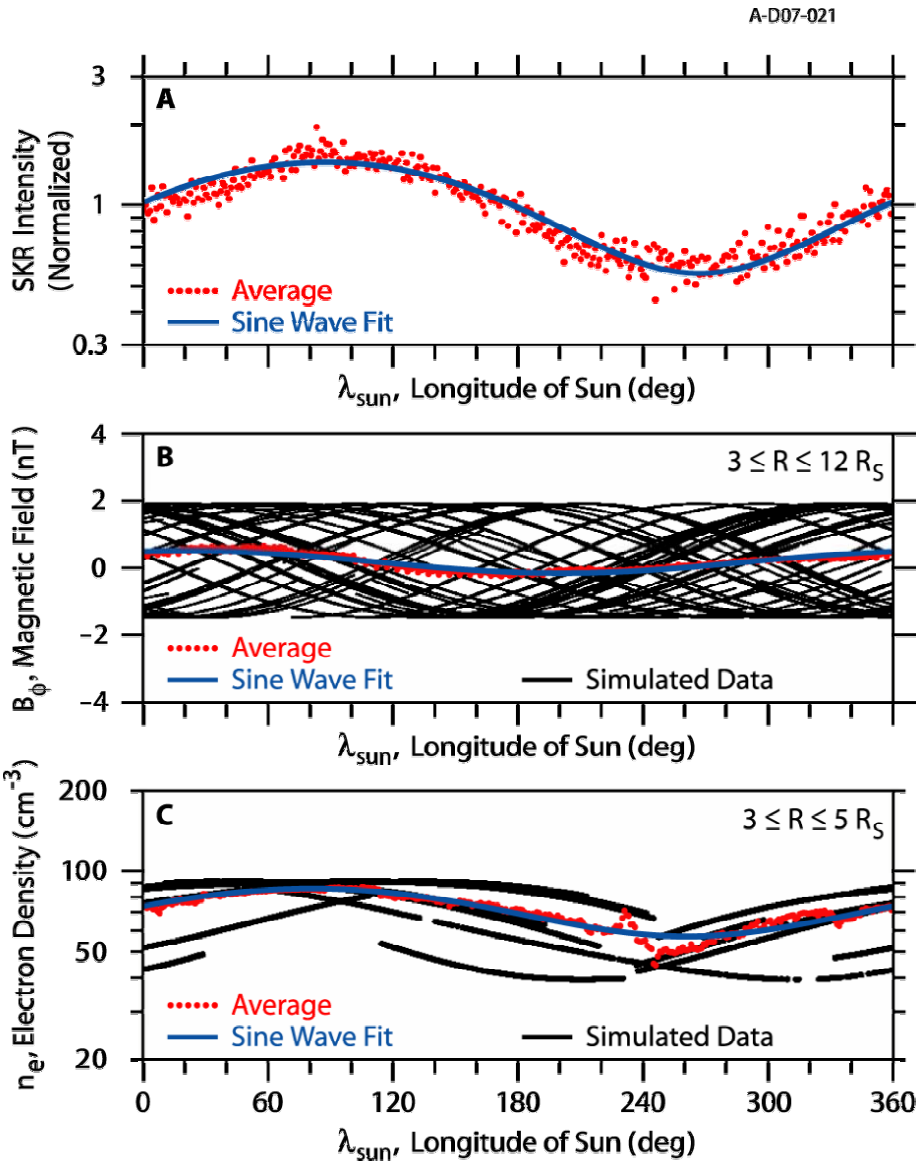

Fig. S5. This plot is again like Fig. 2. However, instead of plotting "real data," in panels (B) an (C) we have plotted "simulated data" derived from the best-fit sine waves (the blue lines) in panels (B) and (C) of Fig. 2. This has been done in order to evaluate the effects of the orbital coverage on the modulation amplitude and spread of the data points relative to the best fit. Comparing the corresponding panels of Figs. S4 and S5, one can see that the modulation amplitudes and spread in the data points between the "real" and "simulated" data are very similar, thereby providing convincing evidence that both the magnetic field and the electron density have a strong rotational control.

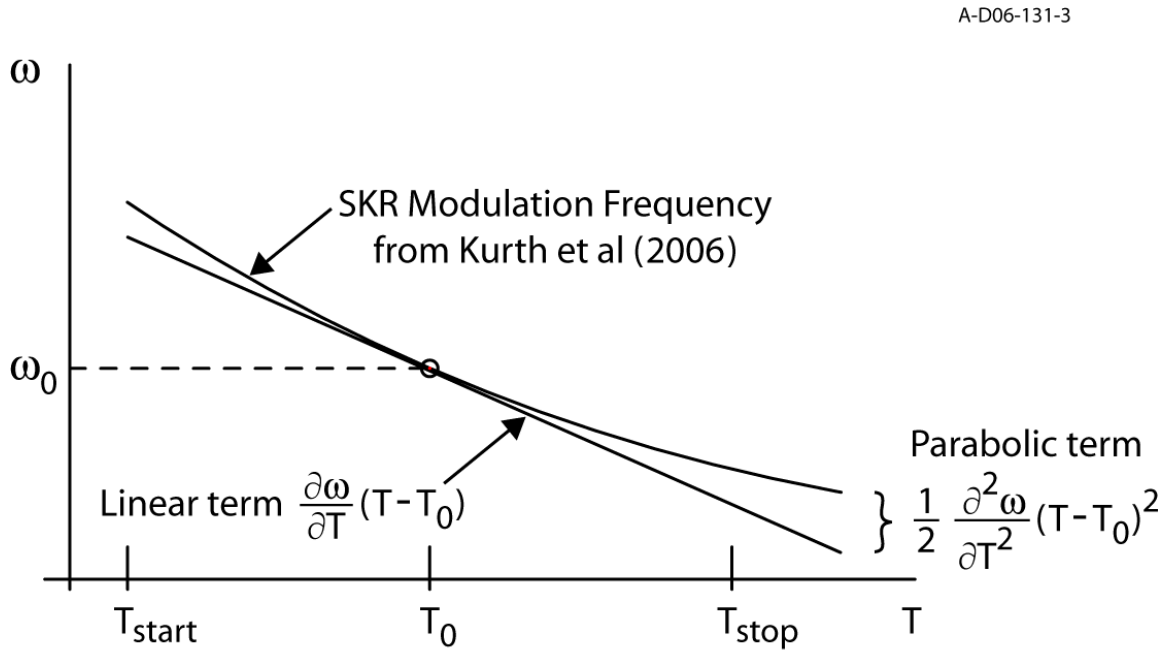

Fig. S6. This plot shows the average modulation frequency of the SKR given by Eq. (S1) as a function of time using the phase correction model of Kurth *et al.* (*S6*). The parameters ω_0, $\partial\omega/\partial t$ and $(1/2)\partial^2\omega/\partial T^2$ are the coefficients of the Taylor series expansion given by Eq. (S1) evaluated at T_0. By evaluating the amplitude of the best-fit sine wave as these parameters are varied one at a time, we can determine the accuracy of the best-fit parameter given by Kurth *et al.,* and also evaluate possible aliasing effects due to data gaps.

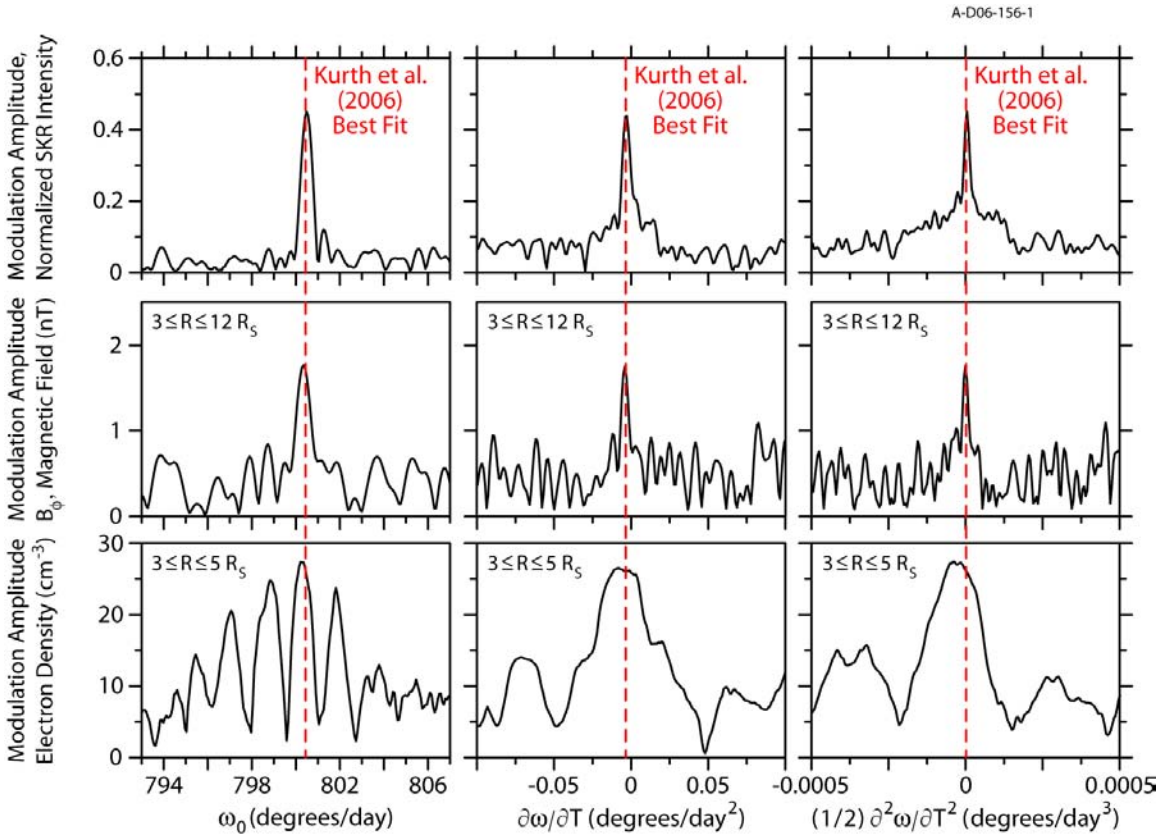

Fig. S7. The results of the parametric analysis of the modulation amplitudes for the three quantities shown in Fig. 2. These plots show the best-fit sine wave modulation amplitudes for three quantities: (1) the normalized SKR intensity in the top row; (2) the B_φ magnetic field in the middle row; and (3) the electron density in the bottom row. These amplitudes are plotted as a function of the Taylor series expansion coefficients, ω_0 in the first column, $\partial\omega/\partial T$ in the second column, and (1/2) $\partial^2\omega/\partial T^2$ in the third column. The vertical red dashed lines indicate the nominal value of these expansion coefficients given by the Kurth *et al.* model evaluated at T_0 = July 1, 2005. The data are from the same orbits used in Figs. 1 and 2. The coincident peaks in the modulation amplitude of the SKR, the magnetic field, and the plasma density, show that all three of these quantities are locked within experimental error to the same time-dependent modulation frequency, as determined by the phase correction term φ(T) given by Kurth *et al.* (*S6*).

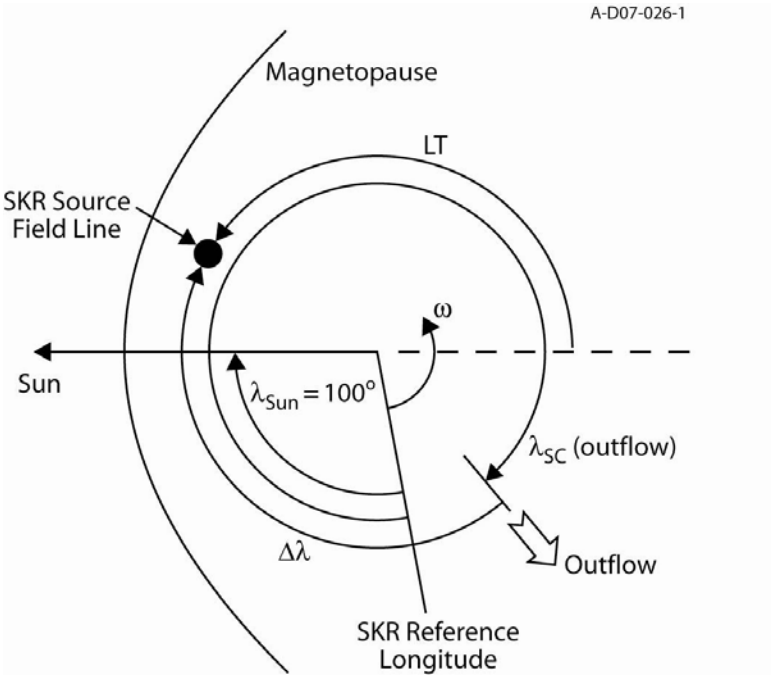

Fig. S8. A diagram showing the phase relationship between the various factors that control the SKR modulation. The diagram is constructed at the time that the SKR reaches peak intensity, i.e., when $\lambda_{Sun} = 100°$. Fig. S3 shows that there is a phase lag of $\Delta\lambda \sim 149°$ to 195° between the longitude where the co-rotating outflow from the convection pattern is believed to originate, λ_{SC}(outflow) ~ 330°, and the longitude, $\lambda_{SC} \sim 119°$ to 165°, at which the disturbance from this outflow reaches the vicinity of the magnetopause at $R \sim 20\ R_S$. From the diagram it can be shown that the corresponding local time of the SKR source is approximately LT ~ 8 to 11 hr, which is consistent with the local time at which the SKR is believed to be generated (*S7, S8*).

References

S1. D. A. Gurnett *et al., Space Sci. Rev.* **114**, 395 (2004).
S2. M. K. Dougherty *et al., Space Sci. Rev.* **114**, 331 (2004).
S3. D. L. Matson, L. J. Spilker, J. – P. Lebreton, *Space Sci. Rev.* **104**, 1 (2002).
S4. D. A. Gurnett, A. Bhattacharjee, *Introduction to Plasma Physics* (Cambridge Univ. Press, Cambridge, 2005), pp. 10-12.
S5. A. M. Persoon, D. A. Gurnett, W. S. Kurth, J. B. Groene, *Geophys. Res. Lett.* **33,** L18106, doi:10.1029/2006GL027090 (2006).
S6. W. S. Kurth, A. Lecacheux, T. F. Averkamp, J. B. Groene, D. A. Gurnett, *Geophys. Res. Lett.* **34***,* L02201, doi:10.1029/2006GL028336 (2007).
S7. A. Lecacheux, F. Genova, *J. Geophys. Res.* **88**, 8993-8998 (1983).
S8. P. Zarka, *J. Geophys. Res.* **103**, 20,159-20,194 (1998).
S9. P. H. M. Galopeau, P. Zarka, D. Le Quéau, *J. Geophys. Res.* **100**, 26,397-26,410 (1995).